PALAEOSTRESS ORIENTATION AND CRUSTAL SHORTENING ESTIMATION, A CASE STUDY FROM THE WRINKLE RIDGES OF NORTHWESTERN PART OF NOACHIS TERRA. K. De[1,2], D. Dasgupta[1], A. Kundu[1], J. Thapa[3], N. Dasgupta[2], [1]Department of Geology, Asutosh College. 92, S.P. Mukherjee Road. Kolkata-700026, West Bengal, India. (de.keyur@gmail.com), [2]Department of Geology, Presidency University. 86/1, College Street. Kolkata-700073, West Bengal, India, [3]Department of Earth Sciences, Indian Institute of Engineering Science and Technology, Shibpur. P.O.- Botanic Garden, Howrah- 711103, West Bengal, India.

Introduction: Wrinkle ridges are hundreds of kilometres long and a few tens of kilometres wide linear features with asymmetric topographic highs with only a few hundred meters elevation. These commonly are asymmetric fault-related folds overlying buried thrust faults [1]. At the north-western corner of Noachis Terra [58˚W, 16˚S to 48˚W, 35˚S] wrinkle ridges trending N-S to NNE-SSW, E-W to ENE-WSW, NW-SE are present (Figure 1). The profiles across the wrinkle ridges,

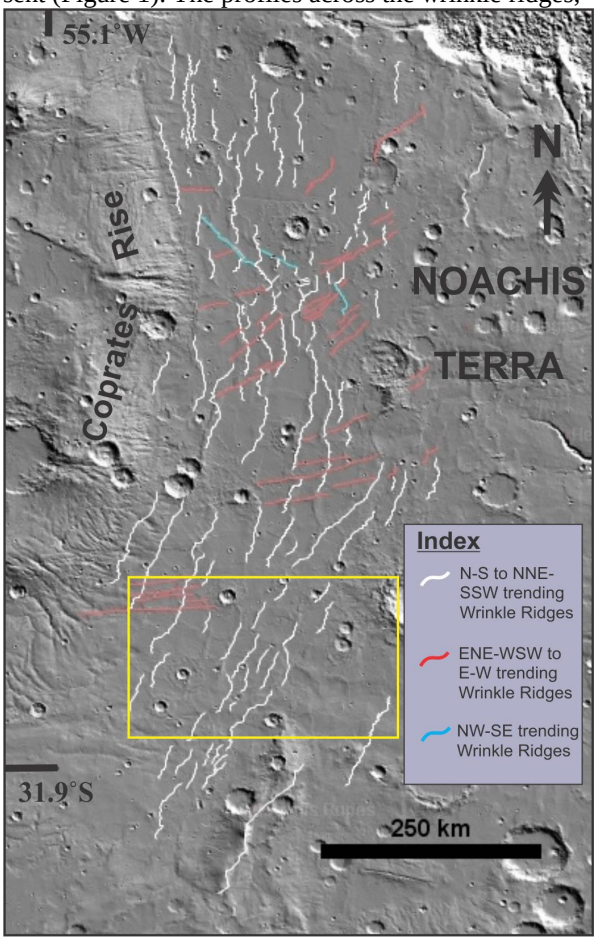

Figure 1. Wrinkle ridges of Northwestern part of Noachis Terra marked on THEMIS Day IR global mosaic [2]. Yellow rectangular box indicates the area of detailed study shown in Figure 3a.

extracted through MOLA DTM [3] (Figure 2a and b), show that almost all have asymmetrical profiles, in which most of them reveal base of western limb of the folds is at higher elevation than that of eastern limb. Many of these wrinkle ridges persist upto a length of ~170kms without any break. These are ~5 to ~17km wide and have an elevation offset of ~20 to ~130m. Consistent orientation of the elevation offsets for

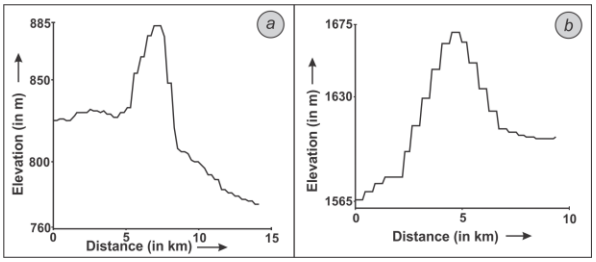

Figure 2. (*a, b*): Example of different wrinkle ridge profiles.

parallel wrinkle ridges suggests that the underlying thrust faults are members of a family that all dip in the same direction. Such consistent wrinkle ridges are therefore favourable features for estimation of palaeostress direction and crustal stortening.

3D Modelling and Palaeostress Analysis: An attempt has been made to make a schematic 3D model to explain the possible structure beneath the NNE-SSW trending wrinkle ridges using the profile sections of a series of four wrinkle ridges (Figure 3a to c). For palaeostress analysis trends of small straight domains,

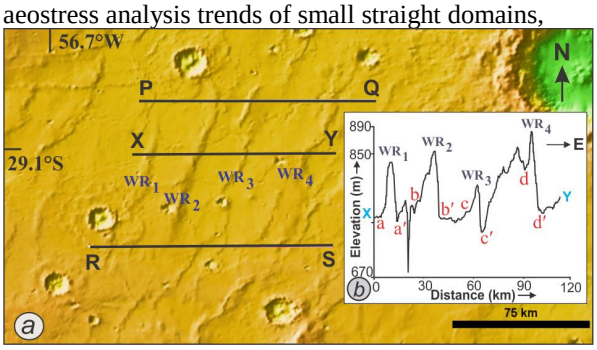

Figure 3. ***(a)*** MOLA DTM image of wrinkle ridges of east of Coprates Planum. PQ, RS are the reference lines where profile sections are extracted to construct a schematic 3D model of the wrinkle Ridges with subsurface structures (Figure 3*c*). ***(b)*** Wrinkle ridge profile extracted from MOLA DTM along XY (Figure 3a).

representing strike of the buried thrusts, and the corresponding dip directions are measured in absence of sub-surface data. Thrusts are considered as dip-slip (i.e., 80˚-90˚ rake of the slip line) with 30˚ slope [cf. 4, 5]. The Fault-line data are projected stereographically

using T-Tecto 3.0 software [6] for slip vector analysis [4, 6] of the wrinkle ridges. A ~ NE-SW directed horizontal maximum principal stress (σ_1) is found to be responsible for the formation of the NNE-SSW trending wrinkle ridges while the minimum principal stress (σ_3) was vertical (Figure 3d).

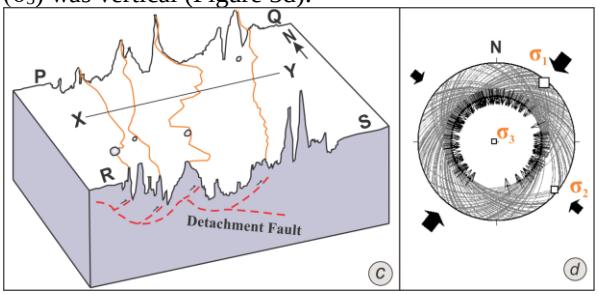

Figure 3. (*c*) Schematic 3D model of the wrinkle Ridges with subsurface structures. ***(d)*** Principal axes of stress (palaeostress) responsible for faulting that developed the NNE-SSW trending wrinkle ridges. The great circles represent the buried faults while arrows indicate slip-lines.

Crustal Shortening and Depth of Detachment Calculation: To estimate the crustal shortening, topographic profiles across four selected wrinkle ridges (WR_1 to WR_4) are constructed (Figure 3b). In earlier works vertical exaggeration is removed for each straight line segment between adjacent nodes on the profile curves and thereby calculating the length [7, 8, 9]. Across a wrinkle ridge, in absence of sub-surface data, only the difference between length of the profile curve and that of the horizontal base between two fixed end points is considered as the extent of shortening. In the present work an easier software based method is used. The profile sections are constructed through the JMARS [10] and vertical exaggeration of the profiles are removed in vector graphics editor software to aquire the new form of the graphs which give the actual lengths of the deformed profile section, representing

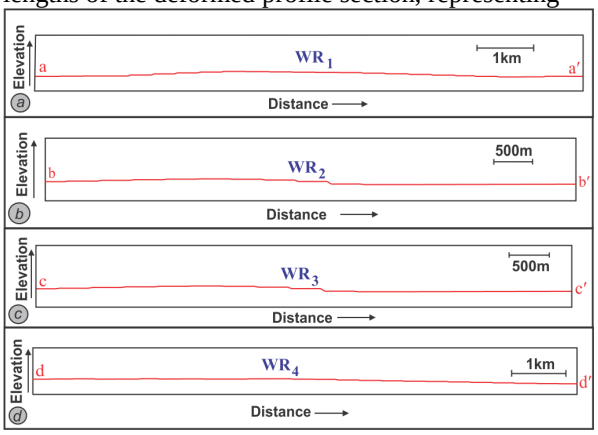

Figure 4. (*a, b, c, d*): Profile section along aa′, bb′, cc′, dd′ (refer to Figure 3 a and b) across a NNW-SSE trending wrinkle ridge after removal of Vertical Exaggeration. Calculated shortening varies from 0.07 to 0.22% (Table 1). In all the graphs, the horizontal length is the final length after shortening (wrinkle ridge formation) and length of the curve is the initial length before shortening.

the initial crustal length and that of the base representing the final crustal length (Figure 4a to d). For NNE-SSW trending wrinkle ridges shortening estimates (Table 1) done by the new procedure adopted in this workare matching with the estimates for Martian and Lunar wrinkle ridges done by other workers [9]. Depth of detachment has been calculated (Table 1) following excess area method [11].

Wrinkle Ridge	Shortening in %	Depth of Detachment (in km)
WR_1	0.22	16.55
WR_2	0.1	38.09
WR_3	0.22	8.35
WR_4	0.07	28.67

Table 1: Shortening and Depth of Detachment values for wrinkle ridges (WR_1 to WR_4; Figure 3a, b, 4a to d).

From this small exercise it can be concluded that a NE-SW trending horizontal compressive stress was responsible for formation of the NNW-SSE striking thrust faults generating the wrinkle ridges. The extent of crustal shortening across these ridges are ~.07% to ~0.22%. The detachment depth varies across the faults. Therefore, it is likely that some of the faults are splays. This also compels us to draw only a sketchy detachment in the model where the faults immediately below the wrinkle ridges are shown.

Acknowledgement: A research grant from Space Application Centre, ISRO is acknowledged.

References: [1] Watters T. R. and Schultz R. A. (2010) *Cambridge University Press*, 183-232. [2] Hill J. et al. (2014) *International Conference on Mars, 8*, 1141. [3] Smith D. et al. (2003) Mars Global Surveyor Laser Altimeter Mission Experiment GriddedData Record. NASA Planetary Data System, MGS-MMOLA-5-MEGDR-L3-V1.0. [4] Ferrill D. A. et al. (2004) *GSA Today, 14*, 10. [5] De K. et al. (2015) *Curr. Sci., 108, 12*, 2156-2159. [6] Žalohar J. (2009) *Department of Geology, SI-1000 Ljubljana, Slovenia.* [7] Golombek M. P. et al. (2001) *JGR, 106*, 23811–23821. [8] Tate A. et al. (2001) *LPSC XXXII*, Abstract #1444. [9] Golombek M. P. et al. (1991) *LPSC XXI*, 679–693. [10] Christensen P.R. JMARS – A Planetary GIS, http://adsabs.harvard.edu/abs/2009 AGUFM IM 22A..06. [11] Marshak S. and Mitra G. eds. (1988) *Prentice Hall.*